Open access • Journal Article • DOI:10.1021/NL303170M

Boron nitride on Cu(111): an electronically corrugated monolayer. — Source link

Sushobhan Joshi, David Écija, Ralph Koitz, Marcella Iannuzzi ...+8 more authors

Institutions: Technische Universität München, University of Zurich, Max Planck Society

Published on: 19 Oct 2012 - Nano Letters (American Chemical Society)

Topics: Boron nitride, Monolayer, Graphene, Scanning tunneling microscope and Borazine

Related papers:

- Boron nitride nanomesh.
- Synthesis of monolayer hexagonal boron nitride on Cu foil using chemical vapor deposition.
- Boron nitride substrates for high-quality graphene electronics
- Large Scale Growth and Characterization of Atomic Hexagonal Boron Nitride Layers
- Monolayer of h-BN chemisorbed on Cu(111) and Ni(111): The role of the transition metal 3d states

Boron nitride on Cu(111): an electronically corrugated monolayer

Joshi, Sushobhan ; Ecija, David ; Koitz, Ralph ; Iannuzzi, Marcella ; Seitsonen, Ari P ; Hutter, Juerg ; Sachdev, Hermann ; Vijayaraghavan, Saranyan ; Bischoff, Felix ; Seufert, Knud ; Barth, Johannes V ; Auwaerter, Willi

Abstract: Ultrathin films of boron nitride (BN) have recently attracted considerable interest given their successful incorporation in graphene nanodevices and their use as spacer layers. to electronically decouple and order functional adsorbates. Here, we introduce a BN monolayer grown by chemical Vapor deposition of borazine on a single crystal Cu support, representing a model system for an electronically patterned but topographically smooth substrate. Scanning tunneling microscopy and spectroscopy experiments evidence a weak bonding Of the single BN sheet to Cu, preserving the insulating character of bulk hexagonal boron nitride combined with a periodic lateral variation of the local work function and the surface potential. Complementary, density functional theory calculations reveal a varying registry of the BN relative to the Cu lattice as origin of this electronic Moire-like superstructure.

DOI: https://doi.org/10.1021/nl303170m

Boron nitride on Cu(111): An electronically corrugated monolayer

Sushobhan Joshi[1], David Ecija[1], Ralph Koitz[2], Marcella Iannuzzi[2], Ari P. Seitsonen[2], Jürg Hutter[2], Hermann Sachdev[3], Saranyan Vijayaraghavan[1], Felix Bischoff[1], Knud Seufert[1], Johannes V. Barth[1] and Willi Auwärter[1]*

[1]Physik Department E20, Technische Universität München, James Franck Str. 1, D-85748 Garching, Germany

[2]Institute of Physical Chemistry, University of Zurich, Winterthurerstr. 190, CH-8057 Zurich, Switzerland

[3]Max-Planck Institut für Polymerforschung, Ackermannweg 10, Mainz, Germany.

ABSTRACT Ultra-thin films of boron nitride (BN) have recently attracted considerable interest given their successful incorporation in graphene nanodevices and their use as spacer layers to electronically decouple and order functional adsorbates. Here, we introduce a BN monolayer grown by chemical vapor deposition of borazine on a single crystal Cu support, representing a model system for an electronically patterned but topographically smooth substrate. Scanning tunneling microscopy and spectroscopy experiments evidence a weak bonding of the single BN sheet to Cu, preserving the insulating character of bulk hexagonal boron nitride, combined with a periodic lateral variation of the local work function and the surface potential. Complementary density functional theory calculations reveal a varying registry of the BN relative to the Cu lattice as origin of this electronic Moiré-like superstructure.

KEYWORDS: hexagonal boron nitride, boron nitride monolayer, insulating layer, borazine, monolayer films, Cu, moiré, STM, interface state, work function, field emission resonance, surface potential, CVD

Atomically thin layers of carbon (graphene) and hexagonal boron nitride (*h*-BN) can be grown on various transition metal supports with exquisite control of the interface structure[1]. In analogy to graphene, a two-dimensional atomically thin boron nitride film is named boronitrene layer or BN

monolayer[2]. These sp^2-hybridized sheets currently attract considerable attention, both for the fascinating properties of the individual monolayers and for the promising characteristics of systems combining graphene and *h*-BN. In case of *h*-BN, the bulk compound has excellent properties like inertness, high temperature stability, low dielectric constant, large thermal conductivity and high mechanical strength[3, 4]. Additionally, crystalline *h*-BN is a 5.97 eV direct band gap insulator and can emit photons in the far-ultraviolet range[5-7]. Thus, ultra-thin layers of boron nitride are promising functional materials. In a nano and surface science context, two applications make BN monolayers highly relevant: First, their combined use with graphene in atomically defined bi- or multilayer heterostructures and second their role as templates to support, decouple and order individual adsorbates or nanostructures. The structural similarity of two-dimensional graphene and *h*-BN expressed by a small lattice mismatch (1.7%)[8] makes *h*-BN a promising substrate for graphene electronics[9]. Indeed the functional characteristics of graphene on *h*-BN are drastically improved compared to conventional SiO_2 substrates.[10-12] Furthermore *h*-BN allows to tune the band gap of graphene in heterostructures [8, 13] or in hybridized single-layer systems[14]. Regarding the use of epitaxial BN monolayers as templates, several recent reports highlight functionalities gained by the decoupling and ordering properties of BN[15-19].

The successful growth of single BN layers by chemical vapor deposition (CVD) or subsequent chemical reactions has been reported e.g. on various 3d, 4d and 5d transition metals[1, 20-24]. Depending on lattice mismatch, symmetry of the supporting surface and interaction strength between BN and metal, a variety of morphologies can be achieved: Uniform commensurate layers (Ni(111))[25-28], films exhibiting Moiré patterns (Pd(111), Pt(111), Pd(110))[29-31], strongly corrugated nanomesh topologies (Rh(111), Ru(0001))[16, 32] or one-dimensional superstructures (Cr(110), Fe(110))[33, 34]. For all the substrates addressed in a recent density-functional theory (DFT) study, the N atom in the BN layer is repelled from the metal while the B is attracted[35]. Accordingly, the registry of the (B, N) units to the surface metal atoms is crucial for the bonding strength. Considerable geometric corrugations can only be achieved by a large lattice mismatch combined with strong electronic BN/metal interactions, which are dictated by the filling of the metal d shell. According to theoretical reports, BN thus has a very low binding energy on Ag(111) and Cu(111), consistent with experimental evidence of a weak interaction in both systems[24, 28]. In analogy to the Ni(111) case, where the small lattice mismatch of -0.4 % leads to a commensurate 1x1 structure[26, 36], a slightly stretched commensurate 1x1 overlayer was proposed for Cu(111) which has a 2.6 % larger lattice constant than Ni(111) [28].

Compared to other transition metal substrates, Cu(111) has so far received very little attention for *h*-BN adsorption. This is surprising, as Cu foils are emerging as highly important substrates for mass production of large scale *h*-BN films[4, 37] which in turn are crucial ingredients in graphene based devices (vide supra)[38]. Here, copper is attractive due to its high purity, relative cheapness and etchability. Consequently, it is of eminent importance to characterize the BN/Cu(111) interface in detail, as it serves as a model system for *h*-BN overlayers on copper. In contrast to the BN case,

graphene growth on Cu single crystals is well documented [39-41].

In this letter, we present a thorough characterization of a BN monolayer grown on Cu(111) by CVD of borazine $(HBNH)_3$ under well-defined ultra high vacuum (UHV) conditions. Using low-temperature scanning tunneling microscopy (STM), spectroscopy (STS) and complementary DFT calculations, we show that a BN monolayer interacts very weakly with the supporting Cu surface and thus keeps its intrinsic insulating properties of *h*-BN. In contrast to previous studies[28], our data evidence a non-commensurate overlayer structure. Importantly, we report a considerable electronic corrugation of the BN monolayer on Cu(111), caused by a mismatch in the registry to the substrate. In contrast to other BN/metal systems, this superstructure is not linked to a strong geometric corrugation. This makes BN/Cu(111) unique.

The initial growth phase of boron nitride on Cu(111) was studied by applying sub-monolayer coverages. Such incomplete layers allow for a direct comparison of BN terminated surface areas with bare Cu(111). Figure 1 shows STM images recorded after exposing the Cu substrate to 42 L of borazine at 980 K. At a sample bias of 4 V BN islands of irregular shape are observed (Fig. 1a). The BN exhibits a Moiré-type corrugation featuring protrusions, labeled “Hills (H)” and depressions, referred to as “Valleys (V)”. At lower bias voltages, the BN appears transparent in STM images and is nearly indistinguishable from the Cu substrate, mainly the island boundaries are discernible (Fig. 1b). The apparent height of the BN layer is plotted in Fig. 1c depending on the sample bias. In a large voltage range ($-4\ V < V_b < 3\ V$) the apparent height is below 0.3 Å, while at 4 V and 6 V it exceeds 4 Å. This clearly indicates that STM images do not reveal the true topographic height of the BN islands, which is close to 3.0 Å (vide infra) but are rather dominated by electronic effects. Indeed, given the insulating property of *h*-BN, we do not expect a contribution of BN to the local density of state (LDOS) within the band gap. Accordingly, the BN islands appear nearly transparent in STM data covering an extended voltage range around the Fermi level (E_F). The large apparent height of BN layers at high positive sample bias voltages, representing unoccupied electronic states, emerges from tunneling into field emission resonances (FER) [42] and will be discussed below. The contrast at high negative bias voltages is tentatively assigned to the valence band of BN (c.f. Fig. S1 in the supporting information).

Images taken in the gap revealing the Cu terraces and step edges underneath the BN islands show that the latter mainly follow the shape of the Cu island they reside on (Fig. 1b). This suggests that the BN facilitates material transport of Cu atoms on the surface at the growth temperature. The BN "rides" on mobile Cu atoms and stabilizes the underlying Cu islands.

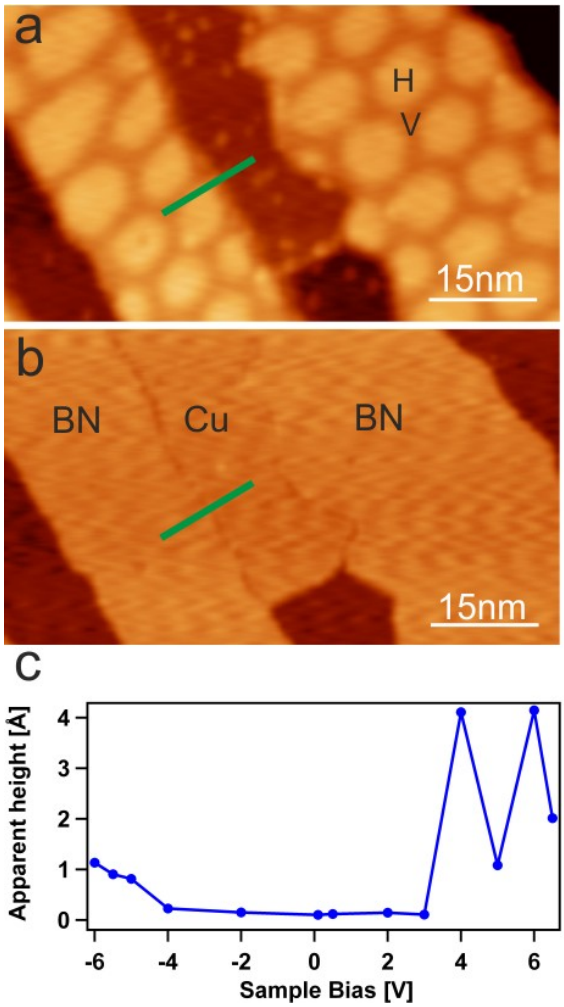

Figure 1. Characterization of BN islands on Cu(111). (a) High-bias STM image of the Cu substrate partially covered by BN. A Moiré-like superstructure distinguishes the BN regions. Here, the bright areas are labeled "Hill (H)" and the surrounding dimmer spaces are named "Valleys (V)" (V_b = 4 V, I = 50 pA). (b) STM image of the same area recorded at lower bias voltage (V_b = 1 V, I = 50 pA). The BN islands are transparent and reveal the underlying Cu(111) terraces. The green line highlights the position used to determine the apparent height of the BN island relative to the Cu(111) support. (c) Averaged apparent height of the BN sub-monolayer as a function of sample bias voltage.

Figure 2a shows a large-scale STM image of a complete BN monolayer on Cu(111) recorded at 4V. As in the sub-monolayer case, the BN is characterized by Moiré patterns. Independent of the preparation conditions (i.e. growth temperature and borazine partial pressure), we always observed the coexistence of such quasi-hexagonal patterns exhibiting different periodicities and orientations (Fig. 2b). However, higher temperature growth of the BN layers seems to increase the domain size. For the highest quality BN film grown at 1120 K altogether thirteen different Moiré patterns with periodicities ranging from 5 nm to nearly 13 nm were identified. Figure 2b shows four of these Moiré domains labeled α, β, γ and δ, respectively. The occurrence and coexistence of Moiré superlattices is well documented for both BN and graphene overlayers on metallic substrates [29, 40, 43], but also for graphite, where so-called supergiant lattices with periodicities up to 15 nm were reported[44]. Generally

the Moiré patterns are caused by a rotational misalignment and/or a different periodicity of the overlayer compared to the supporting lattice [43, 45]. As control experiments omitting the borazine dosage yield a bare Cu(111) surface without any Moiré-like structures, we exclude that graphene islands induced by a potential carbon contamination contribute to the observed surface structures.

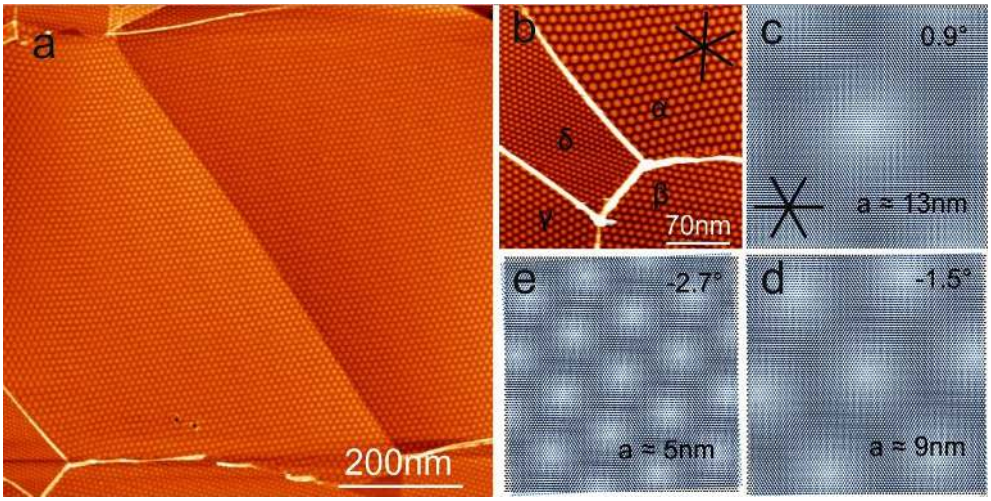

Figure 2. Complete BN monolayer on Cu(111). (a) STM image evidencing coexisting BN domains comprising different Moiré superstructures (V_b = 4 V, I = 40 pA). The central domain extends to the μm range. (b) Enlarged image highlighting four Moiré phases (labeled α, β, γ and δ, respectively) separated by domain boundaries (V_b = 4 V, I = 0.6 nA). Each phase is characterized by a different orientation and periodicity of the pattern. The star represents the dense-packed directions of the Cu(111) lattice. (c-e) Moiré models based on an overlay of two grid patters representing the Cu(111) lattice (black) and a slightly stretched BN overlayer (1% mismatch, blue). Minute misalignment angles below 3° reproduce the full range of periodicities and orientations observed in the experiments. For example the structure presented d) corresponds to the α domain.

To rationalize the emergence and coexistence of the different Moiré patterns, we applied a geometrical model overlay of two hexagonal grids representing the BN and the Cu(111) lattice, respectively. This simple approach proved to be successful in describing Moiré patterns of epitaxial graphene or BN on various transition metal surfaces including Cu(111)[29, 40]. Concerning the BN lattice, it is sufficient to include one atomic species in the modeling, as pointed out in earlier reports[29, 46]. The Cu(111) grid is determined by a lattice constant of 2.556 Å. Neither a rigid BN overlayer with the room-temperature bulk lattice constant of 2.50 Å [47] (2% lattice misfit), nor a BN grid expanded to fit the Cu(111) periodicity (0% lattice misfit) were able to reproduce the experimentally observed Moiré patterns: The periodicity and orientation of the Moiré domains did not match for any rotation angle between the two grids. However, when the BN lattice was slightly stretched (1% lattice misfit) [35], both the measured orientations and periodicities of the Moirés are nicely described by the model overlay applying only minute rotation angles between the two grids. Three cases are highlighted in Fig. 2 c-e

where rotation angles from 0.9° to -2.7° cover the complete range of periodicities observed in the experiments. For example the model in Fig. 2d represents the α domain. The successful description of the experimental data recorded at 6 K by our model relying on a 1% lattice misfit might be attributed to the negative in-plane thermal expansion coefficient of *h*-BN[47] and a deviation of the monolayer lattice constant from the bulk value. Of course this simple model should not be over-interpreted: Experimental data show, e.g. a distortion of the hexagonal symmetry near domain boundaries (see Fig. 2b), indicating some strain in the *h*-BN layer [48]. Nevertheless, it can be concluded that BN on Cu(111) acts neither as a rigid overlayer keeping the bulk lattice constant like on Ag(111)[24] nor does it adapt a commensurate 1x1 structure as on Ni(111) [26]. This finding is in agreement with the observation of randomly oriented triangular BN islands within the same grain of a Cu foil [4] but obviously conflicts with a report claiming a commensurate 1x1 BN monolayer on Cu(111) [28]. This discrepancy might be explained by the coexistence of BN domains exhibiting large periodicities and minute rotation angles could be elusive to LEED observations and only result in broadened integer 1x1 spots.

Figure 3 reveals that the contrast and corrugation of the Moiré patterns drastically depends on the applied bias voltage. Following the trends in apparent height (compare Fig. 1c), the measured corrugation is hardly resolved in a voltage range from -4 V to 3 V (Fig. 3d). At 4 V it reaches a maximum of approximately 1.5 Å, above 4.5 V a contrast inversion is observed, i.e. the regions representing protruding “Hills” at and below 4 V (Fig. 3a) are imaged as depressions above 4.5 V (Fig. 3c). This peculiar behavior is explained by spatial variations of the voltage where the first field emission resonance occurs (vide infra). Importantly, this measurement leads us to conclude that the Moiré patterns are not purely topographic features but instead mainly an electronic effect.

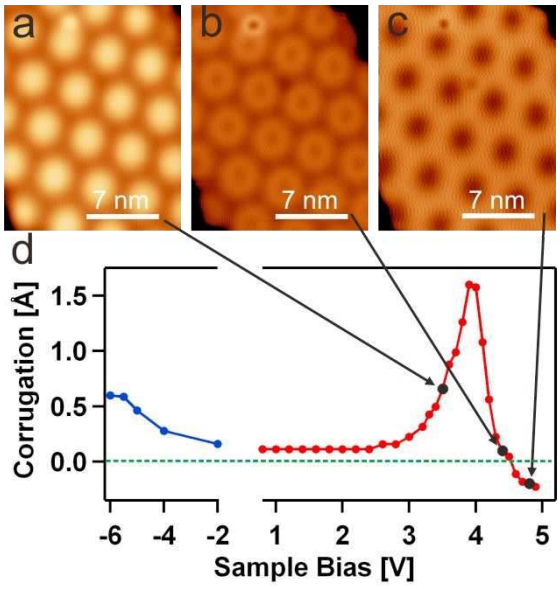

Figure 3. Electronic origin of the Moiré superstructure. (a) In a large bias voltage range, the Moiré is resolved as quasi-hexagonal array of protrusions ("Hills)" in STM images (V_b = 3.7 V, I = 50 pA). (b) Around 4.25 V the contrast changes (V_b = 4.25 V, I = 50 pA). (c) At higher voltages, a contrast inversion is observed: Now the

connecting "Valley" regions appear brighter than the "Hills" (V_b = 4.9 V, I = 50 pA). (d) Plot of the Moiré corrugation vs. sample bias voltage. The apparent corrugation including the contrast inversion is related to the appearance of the first field emission resonance peak (vide infra, compare Fig.5).

An additional feature related to the electronic structure of BN/Cu(111), an electronic interface state, can be probed at low bias voltages, where the BN overlayer appears transparent (compare Fig. 1c). Figure 4a shows an STM image of a Cu region partially covered by a BN island discernible by the characteristic Moiré pattern. Differential conductance (dI/dV) maps recorded at low bias voltages (Fig. 4b) visualize standing wave patterns both on the bare Cu(111) area and on the BN covered region. On Cu they represent the well-known Shockley-type surface state electrons scattered by defects[49], whereas on BN they are assigned to an interface state band[50]. A close inspection of Fig. 4b reveals a larger wavelength of the standing wave pattern under the BN (region marked in green) than on the bare Cu (red region).

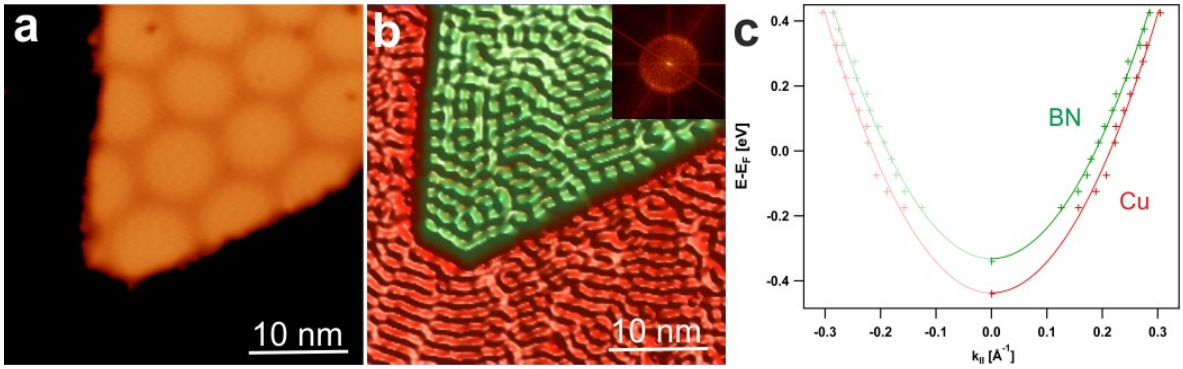

Figure 4. Modification of the Cu(111) surface state upon BN adsorption. (a) STM image of a triangular shaped BN island in Cu(111) (V_b = 4 V, I = 50 pA). (b) dI/dV map of the same area recorded at 0.075 V (I = 0.1 nA). Standing wave patterns are resolved on the bare Cu region (red) and under the BN (green). The wavelength of the BN/Cu(111) interface state is larger than that of the native Cu(111) surface state. The inset shows an FFT image used to extract k_{II}. A comparison to a) reveals that the Moiré features have no discernible impact on the standing wave pattern. (c) The dispersion (E vs k_{II}) of the interface state band (green) reveals an upshift compared to the surface state (red). The data points extracted from dI/dV maps ($k_{II} \neq 0$) and point spectra (k_{II}=0) fit a parabolic dispersion (see text for discussion).

In order to determine the dispersion of the surface and interface state band a series of dI/dV maps was taken in a voltage range from -0.175 V to 0.425 V. For every voltage the wave vector k_{II} was extracted from the fast fourier transform (FFT) of the dI/dV maps for both the bare Cu(111) and the BN regions. A typical FFT image is shown in the inset of Fig. 4b. The resulting dispersion plots (energy versus k_{II}) are displayed in Fig. 4c together with parabolic fits based on the equation $E=E_o+(\hbar k)^2/2m^*$. [51] For the bare Cu(111) area, both the band onset (E_o = -0.44 V) and the effective mass (m^* = 0.40 ± 0.02 m_e) match the literature values [50, 52]. Underneath the BN, the band is clearly upshifted by about 106 meV while the effective mass is hardly changed (m^* = 0.41 ± 0.02 m_e). It is

instructive to compare these values to related systems: A Xe layer adsorbed on Cu(111) induces an upshift of the surface state band of 130 meV [53], for NaCl/Cu(111) a value of 230 meV is reported[50]. This suggests a weak interaction between the BN and the Cu support. More general, according to an empirical rule postulated by Ziroff et al.[54] for physisorbed overlayers, the upshift of the energy (ΔE) can be directly correlated to the adsorption energy per surface area (V_R), with the expression $V_R \propto \Delta E$ using a proportionality constant of 0.106 $Å^{-1}$.[54] Accordingly an energy upshift of 106 meV yields an estimated adsorption energy per surface area of roughly 11.24 meV/$Å^2$ or 59.7 meV/unit cell.

From the perspective of theory, previous studies using density-functional theory (DFT) on a commensurate lattice revealed a strong dependence on the functional employed, e.g. the local-density approximation (LDA) yielded an adsorption energy of 190 meV/unit cell and the generalized gradient approximation (GGA) values as low as 10 meV/unit cell [35]. Our own GGA+vdW calculations include hitherto neglected van der Waals (vdW) contributions and consider a number of different adsorption registries of the BN, focusing on one BN ring (1x1 adsorption). In particular, the strongest binding (with an energy of 270 meV/unit cell) occurs when the B atoms reside in the fcc positions and the N atoms are placed atop Cu atoms in the top layer of the (111) surface ("$B_{fcc}N_{top}$"). The lowest value of the binding energy, 234 meV/unit cell is found for the $B_{fcc}N_{hcp}$ configuration, where both B and N occupy hollow sites (compare Fig. 6). The higher adsorption energies compared to previous results can be rationalized with the use of our vdW correction, which seems to lead to overbinding when compared to the value estimated from the experiments. Looking only at the uncorrected GGA adsorption energies (with unchanged geometries), we find the $B_{fcc}N_{top}$ configuration to be more stable than $N_{hcp}B_{fcc}$ by 120 meV/unit cell. In both cases, however, the adsorption energies are negative (i.e. non-binding), which highlights the importance of our vdW correction.

Both our experimental and calculated adsorption energies indicate that BN has a very weak interaction with the underlying substrate. This supports the findings of earlier DFT calculations[35] claiming that BN/Cu(111) has one of the lowest binding energies as compared to other non-noble transition metals. Clearly, the existence of the diverse Moiré patterns induced by various rotational domains of the BN on Cu(111) is facilitated by this weak interaction. However, it is important to note that the Moiré features have no obvious influence on the interface state standing wave pattern (compare Fig. 4a and b), i.e. we do not observe a quenching of the Shockley surface state at any region. This excludes strong site-specific interactions of the BN with the Cu surface and thus makes a pronounced geometric corrugation of the BN sheet rather unlikely.

As mentioned before, the BN layers appear spatially inhomogeneous due to the presence of Moiré features with predominantly electronic character. To verify the proposed spatial electronic modulation and to characterize the BN in comparison to Cu(111), we performed two sets of experiments yielding information on the surface potential. First, we determined the apparent barrier height ø, which is related to the local work function and thus the surface potential, by measuring the tunneling current *I* as a function of tip sample distance *z*. Figure 5b shows I(Δz) curves representing characteristic locations of the sample indicated in Fig. 5a, namely the bare Cu(111) surface (red), the "Hills H"

(blue) and the "Valleys V" (green) of the BN. The relation $I \propto \exp(-2\kappa z)$, where $\kappa = \sqrt{2m\emptyset}/\hbar$ is the decay coefficient[55], was used to fit the experimental data and to extract κ and ø. [56] This procedure yields the following values: $\kappa_{Cu} = 0.97 \pm 0.02$ Å^{-1}, $\kappa_V = 0.91 \pm 0.02$ Å^{-1} and $\kappa_H = 0.89 \pm 0.01$ Å^{-1}. Hereby, hundreds of I(Δz) curves taken on different, but equivalent locations were averaged. κ_{Cu} agrees reasonably well with previously published values ($\kappa_{Cu} = 1.01 \pm 0.03$ Å^{-1})[56]. Following a protocol discussed by Vitali *et al.*[57] the κ and ø values are used to determine the relative variation of the work function between bare Cu, the "H" and "V" regions, respectively, which is independent from the tip work function. This approximation combined with the reported work function of 4.94 eV for bare Cu(111) [25] yields a work function of 4.1 eV for the BN "V" position and 3.8 eV the "H" locations. Thus, the work function on BN is clearly reduced compared to bare Cu(111), confirming the trends observed at all BN/transition metal interfaces[25]. However, our estimated values based on local measurements indicate a more pronounced shift than inferred from space-averaging methods[28]. Importantly, these results point to a spatial variation of the work function and thus to a variation of the surface potential of the BN monolayer.

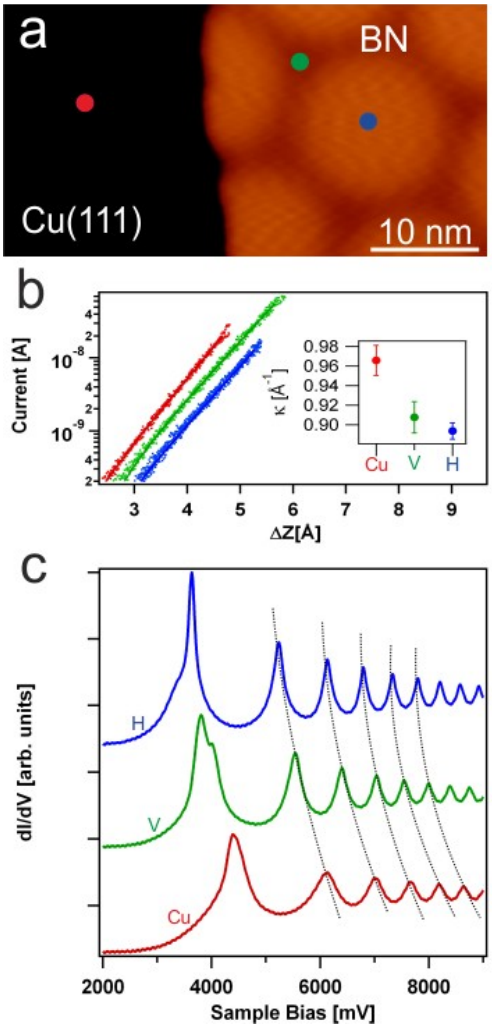

Figure 5. Electronic superstructure of BN/Cu(111). (a) STM image representing the three decisive positions to

characterize the local surface potential at the BN/Cu(111) interface: Bare Cu (red marker), BN Valley (H, green) and BN Hill (H, blue), respectively (V_b = 4 V, I = 50 pA). (b) I(Δz) approach curves at the three points represented in logarithmic scale. The red line exhibits the largest slope followed by green and blue (Curves are laterally offset for clarity). The inset shows the corresponding κ values extracted from the fits in b), reflecting a spatial variation of the local work function. (c) dI/dV spectra showing series of field emission resonances (FERs) representing the same three positions evidence a clear shift in the energy of all resonances, confirming a spatial modulation of the surface potential (see text for discussion). The dashed curves serve as guide to the eye. (Starting parameters: V_b = 1 V, I = 0.1 nA).

To further corroborate this spatial modulation of the electronic structure in BN/Cu(111), we performed a second set of experiments sensing the surface potential. As a probe, we used field emission resonances (FERs). The energies, at which FERs are observed in dI/dV spectra are related to the surface potential, as the FERs are based on image potential states[42]. Figure 5c shows dI/dV traces recorded with closed feedback loop for the three characteristic positions highlighted in Fig. 5a using the very same STM tip. Clearly, a series of well-defined FERs is observed at all location. Importantly, the spectra show significant shifts of all peaks depending on the probed region. As seen in Fig. 5c the first resonance appears clearly above 4 V at the bare Cu(111) (red), below 4 V on the "Valley V" (green) and is shifted to even lower voltages on the "Hills H" (blue). As the first peak of the FERs appears at voltages around the local work function of the sample[58-60], these data confirm a work function lowering on the BN compared to Cu(111) and corroborate the spatial modulation of the surface potential on the BN. Figure 5c also reveals that the appearance of the Moiré patterns, including the observed contrast inversion at high bias voltages (compare Fig. 3), is directly related to the spatial variation of the energy at which the first FER occurs: When increasing the bias voltage, the differential conductance first rises in the "H" area resulting in a larger apparent height of the "Hills" in the STM images. When the bias voltage is augmented further, it matches the energy of the first peak in the "V" region, inducing a bright appearance of the "valley" regions, while the "Hills" appear dim.

In order to model this spatial variation of the electronic landscape theoretically, we studied a 23x23 4-layer Cu(111) slab with an adsorbed 24x24 BN layer which was rotated by 2.11° (further details and results on this system will be published elsewhere). This arrangement leads to a Moiré-type pattern where the adsorption registry spatially varies across the layer with a periodicity of 59 Å. After optimization of the structure the average distance between the monolayer and the surface was 3.0 Å, with a small difference of 0.16 Å between the closest and farthest atoms. Consequently, with BN we present a two-dimensional crystal that interacts only weakly with the Cu(111) support but nevertheless is topographically planar, i.e. withstands instabilities as considerable rippling characteristic for other quasi-freestanding ultra-thin films[64]. The electrostatic potential of the system exhibits spatial variations across this surface, following the change in adsorption registry. In the regions where BN is adsorbed in an $B_{fcc}N_{top}$ fashion, the electrostatic potential (and thus the work function) is 0.13 eV lower than around the $B_{fcc}N_{hcp}$ configuration. In between those two extremes the work function varies in approximately circular patterns. This difference of the work function agrees reasonably well with our experimental estimate, as well as with our results from the 1x1 adsorption, where $B_{fcc}N_{top}$ and $B_{fcc}N_{hcp}$ differ by 0.08 eV. Compared to the bare Cu surface, BN adsorption lowers the calculated work

function by 1.21 eV in the former case, and 1.13 eV in the latter. Fig. 6 summarizes the theoretical findings, comparing the two extreme registries ($B_{fcc}N_{top}$ versus $B_{fcc}N_{hcp}$) of the BN monolayer on Cu(111).

The experimental and theoretical observations outlined above give indications that serve to rationalize the notable electronic corrugation of the BN/Cu(111) system. In particular it is important to appreciate that the electronic corrugation is present even though the monolayer is only very weakly corrugated structurally. It appears that the spatial variation of the adsorption registry is responsible for the modulation of the work function. As BN in the $B_{fcc}N_{top}$ registry interacts stronger with the surface it can change the electronic structure of the substrate, resulting in a stronger lowering of the work function. The small difference in adsorption energy seems to be amplified in the work function. This change of electronic structure is also evidenced by a change in the local density of states of the N atoms, where we observe the highest occupied molecular orbital (HOMO) peak of the p_z states lowered by 0.3 eV in the $B_{fcc}N_{top}$ configuration (see Fig. S1 in the Supporting Information).

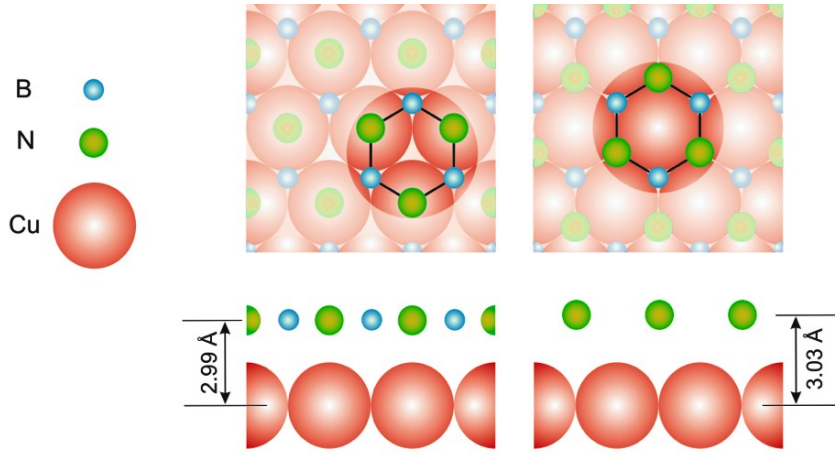

(B , N)	(fcc , top)	(fcc, hcp)
E_{Bind} incl. van der Waals	270 meV / unit cell	234 meV / unit cell
E_{bind} without van der Waals	-171 meV / unit cell	-290 meV / unit cell
Work function; 1 x 1	3.62 eV	3.70 eV
Work function; Moiré	3.64 eV	3.77 eV

Figure 6. Density functional theory calculations of BN/Cu(111). The strongest interaction of the BN with the Cu(111) is observed for a $B_{fcc}N_{top}$ registry, the weakest for $B_{fcc}N_{hcp}$. These two extreme configurations show only minute differences in the adsorption height of the BN, but nevertheless exhibit a markedly different local work function (see text for further discussion).

As shown in various reports a trapping and ordering of atomic or molecular adsorbates can be induced by potential variations across the strongly corrugated BN nanomesh [17, 61-63], in structurally related graphene overlayers [65-68], oxide films [69, 70] or other nanostructured surfaces [71]. Compared to these systems, BN/Cu(111) yields the advantage of being a topographically planar insulating spacer layer. Accordingly, the electronically templated BN monolayer on Cu(111) bears great promise as a

platform for nanoscale assemblies in functional molecular architectures.

In summary, we presented a comprehensive STM/STS study covering the growth and characterization of single BN layers on Cu(111). The insulating properties and the weak interaction of BN with the underlying metallic support are evidenced by the transparent appearance in STM images covering a wide bias range around the Fermi level. The coexistence of various Moiré patterns exhibiting giant periodicities resulting from a minute rotation of BN domains together with the emergence of an electronic interface state band prove a weak binding of the BN monolayer to Cu(111). Different adsorption sites of the slightly stretched BN sheets induce spatial variations in the local work function and thus the surface potential. The resulting electronic superstructure was characterized by exploring lateral modifications of the apparent barrier height and field emission resonances, respectively. Complementary DFT+vdW calculations reveal a planar geometry of the BN sheet on Cu(111) and identify the $B_{fcc}N_{top}$ registry to result in the strongest adsorption energy and lowest local work function. Here, the vdW corrections proved to be decisive for a proper description of the BN adsorption on Cu(111). In conclusion, the electronically templated atomically thin BN layer bears great promise as a platform to support functional nanostructures of reduced dimensions.

ASSOCIATED CONTENT

Supporting Information. Experimental and theoretical details. This material is available free of charge via the Internet at http://pubs.acs.org.

AUTHOR INFORMATION

Corresponding Author

E-mail: (W.A.) wau@tum.de

ACKNOWLEDGMENT

Work supported by the ERC Advanced Grant MolArt (n° 247299), TUM-IAS and the Munich Center for Advanced Photonics (MAP).

References

1. Oshima, C.; Nagashima, A. *J.Phys.: Condens. Matter* **1997,** 9, 1-20.
2. Sachdev, H.; Müller, F.; Hüfner, S. *Diam. Relat. Mat.* **2010,** 19, (7-9), 1027- 1033.
3. Shi, Y.; Hamsen, C.; Jia, X.; Kim, K. K.; Reina, A.; Hofmann, M.; Hsu, A. L.; Zhang, K.; Li, H.; Juang, Z.-Y.; Dresselhaus, M. S.; Li, L.-J.; Kong, J. *Nano Letters* **2010,** 10, (10), 4134-4139.
4. Kim, K. K.; Hsu, A.; Jia, X.; Kim, S. M.; Shi, Y.; Hofmann, M.; Nezich, D.; Rodriguez-Nieva, J. F.; Dresselhaus, M.; Palacios, T.; Kong, J. *Nano Letters* **2011,** 12, (1), 161-166.
5. Zunger, A.; Katzir, A.; Halperin, A. *Phys. Rev. B* **1976,** 13, (12), 5560-5573.
6. Watanabe, K.; Taniguchi, T.; Kanda, H. *Nat. Mater.* **2004,** 3, (6), 404-409.

7. Watanabe, K.; Taniguchi, T.; Niiyama, T.; Miya, K.; Taniguchi, M. *Nat. Photon.* **2009,** 3, (10), 591-594.
8. Giovannetti, G.; Khomyakov, P. A.; Brocks, G.; Kelly, P. J.; van den Brink, J. *Phys. Rev. B* **2007,** 76, (7), 073103.
9. Britnell, L.; Gorbachev, R. V.; Jalil, R.; Belle, B. D.; Schedin, F.; Katsnelson, M. I.; Eaves, L.; Morozov, S. V.; Mayorov, A. S.; M. R. Peres, N. M. R.; Castro Neto, A. H.; Leist, J.; Geim, A. K.; Ponomarenko, L. A.; Novoselov, K. S. *Nano Letters* **2012,** 12, 1707-1710.
10. Dean, C. R.; Young, A. F.; Meric, I.; Lee, C.; Wang, L.; Sorgenfrei, S.; Watanabe, K.; Taniguchi, T.; Kim, P.; Shepard, K. L.; Hone, J. *Nat. Nanotechnol.* **2010,** 5, (10), 722-726.
11. Xue, J.; Sanchez-Yamagishi, J.; Bulmash, D.; Jacquod, P.; Deshpande, A.; Watanabe, K.; Taniguchi, T.; Jarillo-Herrero, P.; LeRoy, B. J. *Nat. Mater.* **2010,** 10, (4), 282-285.
12. Decker, R.; Wang, Y.; Brar, V. W.; Regan, W.; Tsai, H.-Z.; Wu, Q.; Gannett, W.; Zettl, A.; Crommie, M. F. *Nano Letters* **2011,** 11, 2291-2295.
13. Ramasubramaniam, A.; Naveh, D.; Towe, E. *Nano Letters* **2011,** 11, (3), 1070-1075.
14. Ci, L.; Song, L.; Jin, S.; Jariwala, D.; Wu, D.; Li, Y.; Srivastava, A.; Wang, Z. F.; Storr, K.; Balicas, l.; Liu, F.; Ajayan, P. M. *Nat. Mater.* **2010,** 9, 430-435.
15. Muntwiler, M.; Auwärter, W.; Seitsonen, A. P.; Osterwalder, J.; Greber, T. *Phys. Rev. B* **2005,** 71, 241401.
16. Corso, M.; Auwärter, W.; Muntwiler, M.; Tamai, A.; Greber, T.; Osterwalder, J. *Science* **2004,** 303, (5655), 217-220.
17. Berner, S.; Corso, M.; Widmer, R.; Groening, O.; Laskowski, R.; Blaha, P.; Schwarz, K.; Goriachko, A.; Over, H.; Gsell, S.; Schreck, M.; Sachdev, H.; Greber, T.; Osterwalder, J. *Angew. Chem. Int. Ed.* **2007,** 119, (27), 5207-5211.
18. Bose, S.; Garcia-Garcia, A. M.; Ugeda, M. M.; Urbina, J. D.; Michaelis, C. H.; Brihuega, I.; Kern, K. *Nat. Mater.* **2010,** 9, 550-554.
19. Kahle, S.; Deng, Z.; Malinkowski, N.; Tonnoir, C.; Forment-Aliaga, A.; Thontasen, N.; Rinke, G.; Le, D.; Turkowski, V.; Rahman, T. S.; Rauschenbach, S.; Ternes, M.; Kern, K. *Nano Letters* **2012,** 12, 518-521.
20. Auwärter, W.; Suter, H. U.; Sachdev, H.; Greber, T. *Chem. Mater.* **2003,** 16, (2), 343-345.
21. Goriachko, A.; He; Knapp, M.; Over, H.; Corso, M.; Brugger, T.; Berner, S.; Osterwalder, J.; Greber, T. *Langmuir* **2007,** 23, (6), 2928-2931.
22. Sutter, P.; Lahiri, J.; Albrecht, P.; Sutter, E. *ACS Nano* **2011,** 5, 7303-7309.
23. Müller, F.; Hüfner, S.; Sachdev, H.; Gsell, S.; Schreck, M. *Phys. Rev. B* **2010,** 82, 075405.
24. Müller, F.; Hüfner, S.; Sachdev, H.; Laskowski, R.; Blaha, P.; Schwarz, K. *Phys. Rev. B* **2010,** 82, (11), 113406.
25. Nagashima, A.; Tejima, N.; Gamou, Y.; Kawai, T.; Oshima, C. *Phys. Rev. B* **1995,** 51, (7), 4606-4613.
26. Auwärter, W.; Kreutz, T. J.; Greber, T.; Osterwalder, J. *Surf. Science* **1999,** 429, (1-3), 229-236.
27. Auwärter, W.; Muntwiler, M.; Osterwalder, J.; Greber, T. *Surf. Science* **2003,** 545, (1-2), L735-L740.
28. Preobrajenski, A. B.; Vinogradov, A. S.; Mårtensson, N. *Surf. Science* **2005,** 582, (1-3), 21-30.
29. Morscher, M.; Corso, M.; Greber, T.; Osterwalder, J. *Surf. Science* **2006,** 600, (16), 3280-3284.
30. Preobrajenski, A. B.; Vinogradov, A. S.; Ng, M. L.; Cavar, E.; Westerström, R.; Mikkelsen, A.; Lundgren, E.; Mårtensson, N. *Phys. Rev. B* **2007,** 75, (24), 245412.
31. Corso, M.; Greber, T.; Osterwalder, J. *Surf. Science* **2005,** 577, L78-L84.
32. Brugger, T.; Günther, S.; Wang, B.; Dil, J. H.; Bocquet, M.-L.; Osterwalder, J.; Wintterlin, J.; Greber, T. *Phys. Rev. B* **2009,** 79, 045407.
33. Müller, F.; Hüfner, S.; Sachdev, H. *Surf. Science* **2008,** 602, 3467-3476.
34. Vinogradov, N. A.; Zakharov, A. A.; Ng, M. L.; Mikkelsen, A.; Lundgren, E.; Martensson, N.; Preobrajenski, A. B. *Langmuir* **2011,** 28, 1775-1781.
35. Laskowski, R.; Blaha, P.; Schwarz, K. *Phys. Rev. B* **2008,** 78, (4), 045409.
36. Rokuta, E.; Hasegawa, Y.; Suzuki, K.; Gamou, Y.; Oshima, C.; Nagashima, A. *Phys. Rev. Lett.* **1997,** 79, (23), 4609-4612.
37. Song, L.; Ci, L.; Lu, H.; Sorokin, P. B.; Jin, C.; Ni, J.; Kvashnin, A. G.; Kvashnin, D. G.; Lou, J.; Yakobson, B. I.; Ajayan, P. M. *Nano Letters* **2010,** 10, 3209-3215.
38. Bokdam, M.; Khomyakov, P. A.; Brocks, G.; Zhong, Z.; Kelly, P. J. *Nano Letters* **2011,** 11, 4631-4635.
39. Rasool, H. I.; Song, E. B.; Allen, M. J.; Wassei, J. K.; Kaner, R. B.; Wang, K. L.; Weiller, B. H.;

Gimzewski, J. K. *Nano Letters* **2011,** 11, 251-256.
40. Gao, L.; Guest, J. R.; Guisinger, N. P. *Nano Letters* **2010,** 10, (9), 3512-3516.
41. Ogawa, Y.; Hu, B.; Orofeo, C. M.; Tsuji, M.; Ikeda, K.; Mizuno, S.; Hibino, H.; Ago, H. *J. Phys. Chem. Lett.* **2012,** 3, 219-226.
42. Binnig, G.; Frank, K. H.; Fuchs, H.; Garcia, N.; Reihl, B.; Rohrer, H.; Salvan, F.; Williams, A. R. *Phys. Rev. Lett.* **1985,** 55, (9), 991-994.
43. Merino, P.; Svec, M.; Pinardi, A. L.; Otero, G.; Martin-Gago, J. A. *ACS Nano* **2011,** 5, 5627-5634.
44. Xhie, J.; Sattler, K.; Ge, M.; Venkateswaran, N. *Phys. Rev. B* **1993,** 47, (15835-15841).
45. Hermann, K. *J. Phys.: Condens. Matter* **2012,** 24, 314210.
46. Ćavar, E.; Westerström, R.; Mikkelsen, A.; Lundgren, E.; Vinogradov, A. S.; Ng, M. L.; Preobrajenski, A. B.; Zakharov, A. A.; Mårtensson, N. *Surf. Science* **2008,** 602, (9), 1722-1726.
47. Paszkowicz, W.; Pelka, J. B.; Knapp, M.; Szyszko, T.; Podsiadlo, S. *Appl. Phys. A* **2002,** 75, 431-435.
48. Miller, D. L.; Kubista, K. D.; Rutter, G. M.; Ruan, M.; de Heer, W. A.; First, P. N.; Stroscio, J. A. *Phys. Rev. B* **2010,** 81, 125427.
49. Hörmandinger, G. *Phys. Rev. B* **1994,** 49, (19), 13897-13905.
50. Repp, J.; Meyer, G.; Rieder, K.-H. *Phys. Rev. Lett.* **2004,** 92, (3), 036803.
51. Hasegawa, Y.; Avouris, P. *Phys. Rev. Lett.* **1993,** 71, (7), 1071-1074.
52. Reinert, F.; Nicolay, G.; Schmidt, S.; Ehm, D. *Phys. Rev. B* **2001,** 63, 115415.
53. Park, J.-Y.; Ham, U. D.; Kahng, S.-J.; Kuk. Y; Miyake, K.; Hata, K.; Shigekawa, H. *Phys. Rev. B* **2000,** 62, R16341.
54. Ziroff, J.; Gold, P.; Bendounan, A.; Forster, F.; Reinert, F. *Surf. Science* **2009,** 603, (2), 354-358.
55. Ternes, M.; Gonzalez, C.; Lutz, C. P.; Hapala, P.; Giessibl, F. J.; Jelinek, P.; Heinrich, A. J. *Phys. Rev. Lett.* **2011,** 106, (1), 016802.
56. Repp, J. *Dissertation, Freie Universität Berlin,* **2002**.
57. Vitali, L.; Levita, G.; Ohmann, R.; Comisso, A.; De Vita, A.; Kern, K. *Nat. Mater.* **2010,** 9, (4), 320-323.
58. Ruggiero, C. D.; Choi, T.; Gupta, J. A. *Appl. Phys. Lett.* **2007,** 91, (253106).
59. Ploigt, H.-C.; Brun, C.; Pivetta, M.; Patthey, F.; Schneider, W. D. *Phys. Rev. B* **2007,** 76, 195404.
60. Rienks, E. D. L.; Nilius, N.; Rust, H.-P.; Freund, H.-J. *Phys. Rev. B* **2005,** 71, 241404.
61. Dil, H.; Lobo-Checa, J.; Laskowski, R.; Blaha, P.; Berner, S.; Osterwalder, J.; Greber, T. *Science* **2008,** 319, (5871), 1824-1826.
62. Wang, B.; Bocquet, M.-L. *J. Phys. Chem. Lett.* **2011,** 2, 2341-2345.
63. Ma, H.; Brugger, T.; Berner, S.; Ding, Y.; Iannuzzi, M.; Hutter, J.; Osterwalder, J.; Greber, T. *ChemPhysChem* **2010,** 11, 399-403.
64. Geim, A. K.; Novoselov, K. S. *Nat. Mater.* **2007,** 6, (3), 183-191.
65. Pollard, A. J.; Perkins, E. W.; Smith, N. A.; Saywell, A.; Goretzki, G.; Philipps, A. G.; Argent, S. P.; Sachdev, H.; Müller, F.; Hüfner, S.; Gsell, S.; Fischer, M.; Schreck, M.; Osterwalder, J.; Greber, T.; Berner, S.; Champness, N. R.; Beton, P. H. *Angew. Chem. Int. Ed.* **2010,** 49, 1-7.
66. Barja, S.; Garnica, M.; Hinarejos, J. J.; Vazquez de Parga, A. L.; Martin, N.; Miranda, R. *Chem. Commun.* **2010**.
67. N' Diaye, A. T.; Bleikamp, S.; Feibelman, P. J.; Michely, T. *Phys. Rev. Lett.* **2006,** 97, (21), 215501.
68. Zhang, H. G.; Sun, J. T.; Low, T.; Zhang, L. Z.; Pan, Y.; Liu, Q.; Mao, J. H.; Zhou, H. T.; Guo, H. M.; Du, S. X.; Guinea, F.; Gao, H.-J. *Phys. Rev. B* **2011,** 84, 245436.
69. Nilius, N.; Rienks, E. D. L.; Rust, H.-P.; Freund, H.-J. *Phys. Rev. Lett.* **2005,** 95, 066101.
70. Lin, X.; Nilius, N. *J. Phys. Chem. C* **2008,** 112, 15325-15328.
71. Ruffieux, P.; Ait-Mansour, K.; Bendounan, A.; Fasel, R.; Patthey, F.; Gröning, P.; Gröning, O. *Phys. Rev. Lett.* **2009,** 102, 086807.